Title

Recombinant AMP/Polypeptide Self-Assembled Monolayers with Synergistic Antimicrobial Properties for Bacterial Strains of Medical Relevance

Authors

Sergio Acosta†, Luis Quintanilla†, Matilde Alonso†, Conrado Aparicio‡, José Carlos Rodríguez-Cabello†*

Affiliations

†Bioforge lab, CIBER-BBN, Edificio LUCIA, University of Valladolid, Paseo Belén 19, 47011 Valladolid, Spain

‡ MDRCBB, Minnesota Dental Research Center for Biomaterials and Biomechanics, University of Minnesota, 16-250A Moos Tower, 515 Delaware St. SE, Minneapolis, MN 55455, USA

KEYWORDS: Antimicrobial peptides, self-assembled monolayers, recombinant, elastin-like recombinamers, anti-biofilm

Abstract

Nosocomial infections are one of the most frequent causes of indwelling biomedical device failure. In this regard, the use of antibiofilm nanocoatings based on antimicrobial peptides (AMPs) is a promising alternative to prevent multiresistant biofilm infections. However, the limitations of chemical production impede the large-scale development of advanced antimicrobial materials that improve the properties of AMPs. Herein, we present a multifunctional modular design for the recombinant coproduction of self-assembled monolayers (SAMs) based on AMPs and elastin-like recombinamers (ELRs), which combine the antimicrobial properties of a designer AMP, GL13K, and low-fouling activity of an ELR in a synergistic manner. The inclusion of a grafting domain intended for oriented tethering onto surfaces allowed the recombinant polymers to be covalently immobilized onto model gold surfaces. The antibiofilm properties against two of the bacterial strains most frequently responsible for indwelling medical device-associated infections, namely *Staphylococcus epidermidis* and *Staphylococcus aureus*, were then evaluated. GL13K peptide was found to provide antibiofilm properties to the surface, with these being synergistically enhanced by the antifouling effect of the ELR. This new design offers a promising tool for the development of advanced AMP-based nanocoatings for medical devices with powerful and enhanced features.

Introduction

The aging of the population combined with technological developments in the field of biomaterials have resulted in the increasing use of biomedical devices. However, the implantation of temporary or permanent medical devices implicitly increases the risk of bacterial infections. [1] Indeed, biofilm-related infections and the increasing appearance of multidrug resistant bacteria make medical device-associated infections a significant economic and medical concern. [2,3] Although a wide range of bacteria are implicated in such infections, staphylococci, especially *Staphylococcus aureus* and *Staphylococcus epidermidis*, are of particular importance. Indeed, *S. aureus* and *S. epidermidis* are the leading cause of reported healthcare-associated infections and tare particularly relevant in indwelling device-associated infections due to their ability to form biofilms, their prevalence and the occurrence of multi-drug resistant phenotypes.[4,5]

Significant efforts have been made to design bactericidal and anti-fouling coatings to prevent bacterial adhesion and inhibit biofilm formation on biomaterials,[6,7] including antimicrobial agent releasing-based, anti-fouling and contact-killing coatings. Traditional antibiotics,[8] metallic nanoparticles, such as Ag [9] or Zn, [10] and polymers[11] are the most widely used approaches and have proved effective against staphylococcal strains, although with significant limitations, such as antibiotic resistance, [12] toxicity at high concentrations, [13,14] and lack of biocompatibility. [15] As such, the use of antimicrobial peptides (AMPs) has increased markedly in recent years given their broad-spectrum activity against bacteria, fungi, viruses and parasites, low systemic toxicity and their reduced risk for antimicrobial resistance.[16] AMPs are small amphiphilic peptides (12-50 amino acids) that are usually positively charged and are able to self-assemble [17] and interact with multiple cellular components from both the infectious agent and the host. They also have immune-modulating properties.[18] Consequently, they have been

employed to develop antibiofilm coatings, thereby demonstrating their potential applicability for the prevention of indwelling device-associated infections. AMPs have been directly immobilized onto biomedical materials[19–23] or bioconjugated with a polymeric scaffold that may improve their antimicrobial activity,[24–26] and they can also incorporate additional functionalities such as low-fouling behavior,[27,28] multiple and synergistic antimicrobial peptides[29] or an ability to promote tissue integration.[30,31] Furthermore, the immobilization of AMPs may improve some of their limitations, minimize their toxic side effects and improve their susceptibility to proteases.[32]

The main limitation for the production and improvement of AMP-based coatings for clinical materials is the high cost of chemical manufacture, which impedes scale-up. [33] As such, the recombinant production of AMPs has been studied and several examples have been produced using this methodology. [34,35] Despite this, the recombinant production of AMPs usually involves the use of expensive chromatographic and nonchromatographic techniques for purification of the final product that increase final costs, thereby hampering large-scale production. [36,37] In this regard, and because of their thermosensitive behavior, elastin-like recombinamers (ELRs) enable the efficient recombinant production and simple purification of heterologous proteins in a cost-effective scalable process. [38,39] In addition, chimeric AMP coproduction with ELRs delivers highly monodisperse and pure products and, most importantly, enables the synthesis of sophisticated antimicrobial designs with improved properties and applications by taking advantage of the elastin-like smart behavior and their potential complex molecular architecture. Examples of the latter are films for wound healing [40] and self-assembling antimicrobial nanoparticles. [41] Thus, ELRs and recombinant smart polymers are an attractive alternative for the development of advanced antimicrobial materials for biomedical applications.

To the best of our knowledge, recombinant self-assembled monolayers (SAMs) with antibiofilm and extracellular matrix mimicking properties have not yet been developed for preventing infection in implantable devices. In this study, we aim to produce multifunctional SAMs in which the antibiofilm properties of an AMP are enhanced upon combination with an ELR. Poly-VPGVG matrices and coatings have been shown to exhibit protein antifouling activity. [42–44] Thus, an ELR backbone based on poly-VPGXG (X = V and K in a 5:1 ratio) was designed to provide antifouling properties and a polycationic environment for the AMP to enhance its antimicrobial properties. The AMP cloned and coproduced with the ELR was GL13K, a bioinspired AMP derived from parotid secretory protein (BPIFA2) with high bactericidal potential and antibiofilm activities in solution and on surfaces.[20,22,45] Finally, a C-terminal grafting-motif based on two consecutive cysteines has been incorporated into the ELR design. Cysteine side-chains have demonstrated that are excellent candidates for the selective covalent and functional immobilization of peptides and proteins onto multiple surfaces and biomedical materials for the biofabrication of surfaces with antimicrobial properties,[46,47] cell adhesion selectivity,[48,49] or enzymatically active.[50] Furthermore, due to the extreme versatility of recombinant materials, the modular design (AMP, ELR or grafting domain) is easily editable and other functional groups could be inserted.

To test the antibiofilm activity of the ELR (AM-ELR) as covalent coatings, the ELRs were immobilized onto model gold surfaces and two staphylococcal single-strain biofilm models (*S. aureus* and *S. epidermidis*.) were tested. Strong antibiofilm activity and cytocompatibility of these coatings was demonstrated, thus confirming the potential of recombinant approaches for the production of antimicrobial coatings with powerful features for biomedical devices.

Materials and Methods

Bacteria Strains

The biofilm-producing staphylococcus strains *S. aureus* ATCC 25923 and *S. epidermidis* ATCC 35984 were provided by the American Type Culture Collection (ATCC).

ELR Design

All ELRs used in this study are based on a multimodular design. The first ELR, referred to as VC and used as control, comprises two modules, namely a polycationic backbone $(VPGXG)_{40}$ (where X is Val and Lys in a 5:1 ratio) and a cysteine-based C-terminal grafting domain for covalent immobilization onto surfaces (Table 1). The AM-ELR, referred to as GVC, incorporates this grafting domain and the AMP GL13K[45] at its N-terminus via a flexible linker comprising ten glycines. This Gly linker gives flexibility to allow interaction with the bacterial targets.[51] Polycationic ELRs provide a positive environment, and C-terminal attachment of AMPs increases their antimicrobial potential [52] while minimizing cytotoxic side reactions.[53]

The GVC recombinamer was produced as an EGVC, with a sacrificial block (E) being included immediately before the GL13K sequence as part of the modular design. This E block plays a crucial role for the following reasons: (A) it protects host bacteria during bioproduction by avoiding AMP-associated toxic effects; (B) it contains a methionine at its C-terminus, thus allowing it to be cleaved and releasing the GVC recombinamer in a cost-effective and scalable process and with no extra amino acid that could interfere with the biological properties; (C) it is polyanionic (Table 1), thus meaning that, after cleavage, it can easily be separated from the final product (GVC) by inverse transition cycling (ITC)

in a single step; [54] and (D) it enables separation of the uncleaved original product (EGVC) using the same method.

Table 1. Antimicrobial Peptide and Elastin-Like Recombinamer Sequences.

	Sequence	Mw (Da)
GL13K	GKIIKLKASLKLLC-NH_2	1528.02
VC	MESLLPVG(VPGVGVPGKG$(VGPVG)_4)_8$VCC	21038.0
GVC	GKIIKLKASLKLLVLG_{10}L VG(VPGVGVPGKG$(VGPVG)_4)_8$VCC	22670.0
EGVC	MESLLP$(VGPVG)_2$VPGEG$(VGPVG)_2$VLG_{10}LVMGKIIKLKASLKLLVL G_{10}L VG(VPGVGVPGKG$(VGPVG)_4)_8$VCC	45241.3

AMP/ELR/AM-ELR: Synthesis and Characterization

Recombinamers VC and EGVC were designed and cloned into a pET-25b (+) vector in *E. coli* XL1 Blue Competent cells (Agilent, USA). The gene encoding for the GL13K peptide was synthesized by NZYTech (Portugal). Recombinamer expression and production was performed in an *E. coli* BLR as described elsewhere. [55] After bacterial fermentation in a 15 L bioreactor (Applikon Biotechnology, USA), the ELRs were purified (Figures S1A and S2) by ITC in high yields (190 and 270 mg/L for VC and EGVC, respectively) dialyzed (12,000 MwCO – Medicell Membranes Ltd., UK), filtered (0.22 μm Nalgene, ThermoFisher Scientific), lyophilized and stored at −20 °C.

The monodispersity and purity of the ELRs were assessed by sodium dodecyl sulfate–polyacrylamide gel electrophoresis (SDS-PAGE) and matrix assisted laser desorption/ionization time-of-flight (MALDI-TOF) mass spectrometry. The amino acid composition was checked by high performance liquid chromatography (HPLC; Figures S1 and S2 and Tables S1 and S2).

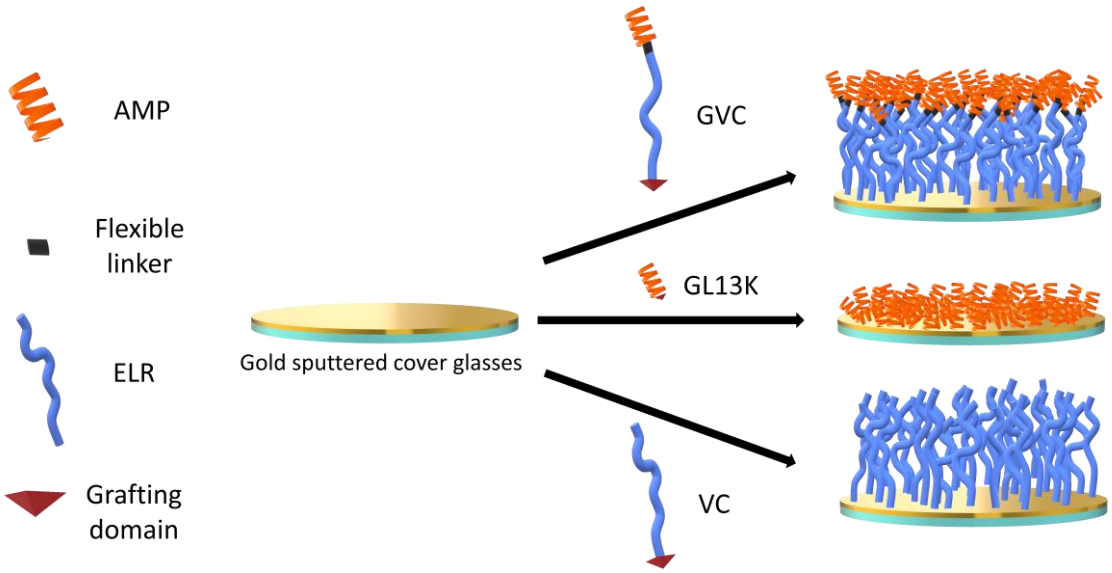

Figure 1. Schematic representation of the modular composition of the AM-ELR and production of the AMP/ELR/AM-ELR self-assembled monolayers (SAMs) on gold surfaces.

EGVC Cleavage

After production and characterization of the EGVC recombinamer (Figures S1 and S2), he sacrificial block (E) was cleaved by treatment with CNBr under acidic conditions (70% formic acid, FA) for 20 h at room temperature to release the GVC recombinamer. The solution was then dried in a rotary evaporator, resuspended in ultrapure water and dialyzed. As a result of the aforementioned diverse physicochemical properties of the sacrificial block and the GVC, said block and the uncleaved EGVC were precipitated in a single centrifugation step (40 °C, pH < 4 and NaCl 0.5 M). The GVC was therefore completely purified in the supernatant (Figure S1B, C), which was dialyzed, filtrated, lyophilized and stored at -20 °C.

Peptide Synthesis

The peptide GL13K was produced by Pepscan (Netherlands) with a purity of more than 92%. An extra Cys was incorporated at the C-terminus for subsequent oriented attachment to gold surfaces.

Preparation of SAMs

To study the AM-ELR as a covalent coating, GL13K, VC, and GVC were covalently immobilized onto model gold surfaces (Figure 1) via the Cys residues present in the AMP/ELR/AM-ELR.[56] To prepare the gold surfaces, cover glasses with a diameter of 12 mm (ThermoScientific) were cleaned with Argon plasma for 15 min at a high power setting (29.6 W applied to the RF coil) using a PDC-002 plasma cleaner (Harrick Plasma, USA). These cover glasses were then covered with a 40 nm gold layer using a sputter coater (Emitech K575X) with a gold layer with a purity of 99.99% (150 s, 30 mA). The resulting surfaces were immediately immersed in 200 μM AMP/ELR/AM-ELR solutions for 4 h, then washed three times with ultrapure water and ethanol to remove physisorbed molecules, dried under vacuum overnight and stored at −80 °C for further use.

Characterization of the Coatings

Water Contact Angle (WCA)

Water contact angle measurements were performed using an OCA 15plus instrument (DataPhysics, Germany) equipped with a CCD camera. At least 10 drops of ultrapure water (0.5 μl) were analyzed per group. All images were collected after stabilization 15 for seconds, and the left and right angles were averaged.

X-ray Photoelectron Spectroscopy

An X-ray Photoelectron K-Alpha (ThermoScientific, USA) spectrometer (SSTTI, University of Alicante, Spain) was used to analyze the sample surfaces. Monochromatic Al–K radiation (1486.6 eV) was employed to collect all spectra, with an elliptical X-ray spot (major axis length of 400 μm) at 3 mA x 12 kV. The alpha hemispherical analyzer was operated in constant energy mode with survey scan pass energies of 200 eV to

measure the whole energy band and 50 eV in a narrow scan to selectively measure the particular elements (C 1s, N 1s, O 1s and Au 4f). XPS data were analyzed using Avantage software. A smart background function was used to approximate the experimental backgrounds, and surface elemental compositions were calculated from background-subtracted peak areas. Charge compensation was achieved using the system flood gun, which provided low-energy electrons and low-energy argon ions from a single source.

Quartz Crystal Microbalance with Dissipation (QCM-D)

The QCM-D technique was applied to estimate the thickness of the covalent coatings. [57,58] This technique allows simultaneous measurements of both frequency and energy-dissipation changes, which were recorded up to the 13th overtone number.

A Q-Sense Explorer System equipment (Biolin Scientific, Sweden) was used. Each solution was pumped with a peristaltic pump through the circular flow circuit at 20 μL/min. All tests were performed at 23 °C.

An AT-cut 5 MHz gold-coated quartz crystal with an estimated surface roughness of 1 nm, according to the manufacturer's technical specifications, was used as sensor (QSX301 Gold, Biolin Scientific) The sensors were cleaned with Argon plasma in a plasma cleaner (using the same parameters indicated in section 2.5) for 5 min immediately prior to use.

The following sequence of flows (or events) was applied in each QCM-D measurement. First, since the AMP/ELRs solutions were prepared in ultrapure water, ultrapure water was passed through the chamber for 2 min to define a stable baseline, followed by the AMP/ELR solution (200 μM) for 25 min, and a final rinse with ultrapure water for 20 min. Three replicates were performed for each measurement.

The QCM-D experimental data were numerically fitted to the Voigt (continuous) viscoelastic model using Dantzig's Simplex algorithm,[59] as implemented in the software from Biolin Scientific (Q-Sense Dfind). An explicit consideration of the frequency dependence of viscoelastic properties was assumed according to a power law. A descending incremental fitting was used, with the quality of the fitting being determined by the parameter χ^2 (lower χ^2 values indicate a better fitting). A χ^2 value of less than 2 was always obtained in the numerical fittings.

Antistaphylococcal Assays

To evaluate the antibiofilm properties of the coatings, two single-strain biofilm models were studied. Thus, the covalently coated surfaces were sanitized with UV light for 30 min/side and staphylococcal biofilms were grown on them. For this, 3–5 colonies from a fresh plate of *S. aureus* ATCC 25923 and *S. epidermidis* ATCC 35984 were inoculated in LB broth medium (Formedium) and incubated aerobically overnight at 37 °C and 200 rpm. The surfaces were then incubated for 24 h (37 °C, 60 rpm, aerobically) with a 1×10^6 CFU/mL inoculum prepared from the overnight preinoculum in fresh TSB medium (Oxoid, tryptic soy broth medium) with (extra) glucose (1%) to induce the adherent phenotype of the staphylococci.[60]

Fluorescence Microscopy: Live/Dead Staining

After incubation, the surfaces were washed gently with NaCl (0.9%) to remove the unattached bacteria and the biofilms were evaluated by fluorescence microscopy. Samples were stained using the LIVE/DEAD BacLight Bacterial Viability kit (Thermo Fisher Scientific, USA) following the manufacturer's instructions, then mounted on a glass sheet and visualized using a Nikon Eclipse Ti E microscope.

Scanning Electron Microscopy (SEM)

After removal of unattached bacteria, the biofilms formed were immobilized on the surfaces as described elsewhere [61] and morphological visualization by SEM was performed. Briefly, the surfaces were incubated in a primary fixation solution (2.5% glutaraldehyde and 0.15% Alcian blue in 0.1 M phosphate buffer (PB), pH 7.4, for 60 min). After washing the surfaces in 0.1 M PB, a secondary fixation solution was employed (1% OsO_4 in 0.1 M PB, 60 min). The samples were then washed and dehydrated in graded ethanol solutions (50%, 70%, 80%, 95% and 100%), critical point dried (Emitech K850) and coated with a 50 Å gold layer using a sputter coater (Emitech K575X). Finally, SEM visualization was carried out using an environmental scanning electron microscope (ESEM) FEI-Quanta 200 Field Emission Gun.

Antibiofilm Activity Quantification: Crystal Violet and ATP Assay

Antibiofilm activity was quantified by combining two different techniques. Thus, crystal violet (CV) dye was used to stain the remaining total biomass and the metabolic activity was evaluated by total ATP quantification. In brief, after bacterial incubation the surfaces were rinsed gently with 0.9% NaCl in a 24-well plate. Each surface was incubated in a 0.1% solution of CV for 15 min at RT, rinsed 4 times with deionized water and dried at RT overnight. Acetic acid solution (30%) was employed to solubilize the CV from the surfaces and the dye was quantified in a 96-well plate by measuring the absorbance at 590 nm using a SpectraMax M2e microplate reader (Molecular Devices, USA). If the absorbance was too high ($Abs^{590} > 1$) the solubilized CV solution was diluted with ultrapure water and the corresponding dilution factor was applied. The metabolic activity was measured by quantifying ATP using the BacTiter-Glo kit (Promega). To that end, after rinsing the coatings, 330 μL of the kit solution was added to a 24-well plate and the

coatings were incubated for 5 min in the darkness, then a 100 μL aliquot was transferred into a white 96-well plate and the luminescence measured using a SpectraMax L microplate reader (Molecular Devices).

Cytocompatibility Assay

The cytocompatibility of the coatings was tested using human foreskin fibroblast (HFF-1) cells, which were purchased from Life Technologies S.A. (Madrid, Spain). To that end, 5000 cells/cm^2 were seeded onto the UV-sanitized surfaces in DMEM medium supplemented with 15% FBS and 100 U/mL to 100 μg/mL penicillin-streptomycin at 37 °C and 10% CO_2. HFF-1 cells at passages between 5 and 8 were employed in all experiments. Cytocompatibility levels were determined using the AlamarBlue (AB) Cell Viability reagent (Thermo Fisher Scientific, USA). Thus, according to the manufacturer's instructions, after the desired incubation times (5 h, 48 h, and 7 days) the surfaces were incubated for 4 h at 37 °C with a 10% AB solution in culture medium and the fluorescence recorded using a SpectraMax M2e microplate reader (Molecular Devices).

Statistical Analysis

A one-way analysis of variance table (ANOVA) with posthoc multiple comparison Holm-Sidak test was used to evaluate the data and intergroup differences using Statgraphics XVII. A *p*-value of less than 0.05 was considered to be statistically significant (****$p < 0.0001$, ***$p < 0.001$, *$p < 0.05$). Results are shown as mean ± standard deviation (SD) ($n \geq 3$).

Results and Discussion

SAMs Biofabrication and Characterization

In this study, antimicrobial nanocoatings for staphylococci biofilm infections, the most frequent cause of biomedical device-associated infections, [62] were recombinantly produced based on the AMP GL13K and an ELR. After covalent attachment of the GVC recombinamer and controls (GL13K and the VC recombinamer) to model gold surfaces, the surfaces were characterized by WCA, XPS, and QCM-D. Physical and chemical characterization was performed, measuring the coating wettability by WCA and quantifying the elemental composition by XPS, respectively. Finally, to assess the effectiveness of AMP/ELR deposition, we used QCM-D to obtain the thickness of the coatings.

The wettability of the coatings was assessed by measuring the static contact angle of ultrapure water drops on the surfaces with a stabilization time of 15 s. The wettability of pristine gold surfaces (WCA = 76.4 ± 2.5°) decreased after being coated with immobilized GL13K peptides (WCA = 85.6 ± 3.8°) (Figure 2). The hydrophobicity of the surface increased as the hydrophobic residues of these amphipathic peptides became exposed at the solid/air interface. [20] The VC recombinamer, in contrast, is a hydrophilic cationic molecule, therefore the VC coatings showed higher wettability (WCA = 58.6° ± 3.4°) than pristine gold and GL13K-coated surface. However, due to the presence of the GL13K peptide, GVC coatings were slightly more hydrophobic than VC coatings (WCA = 67.5° ± 3.1°), thus indicating that GL13K folds and exposes its hydrophobic residues at the solid/air interface. [17]

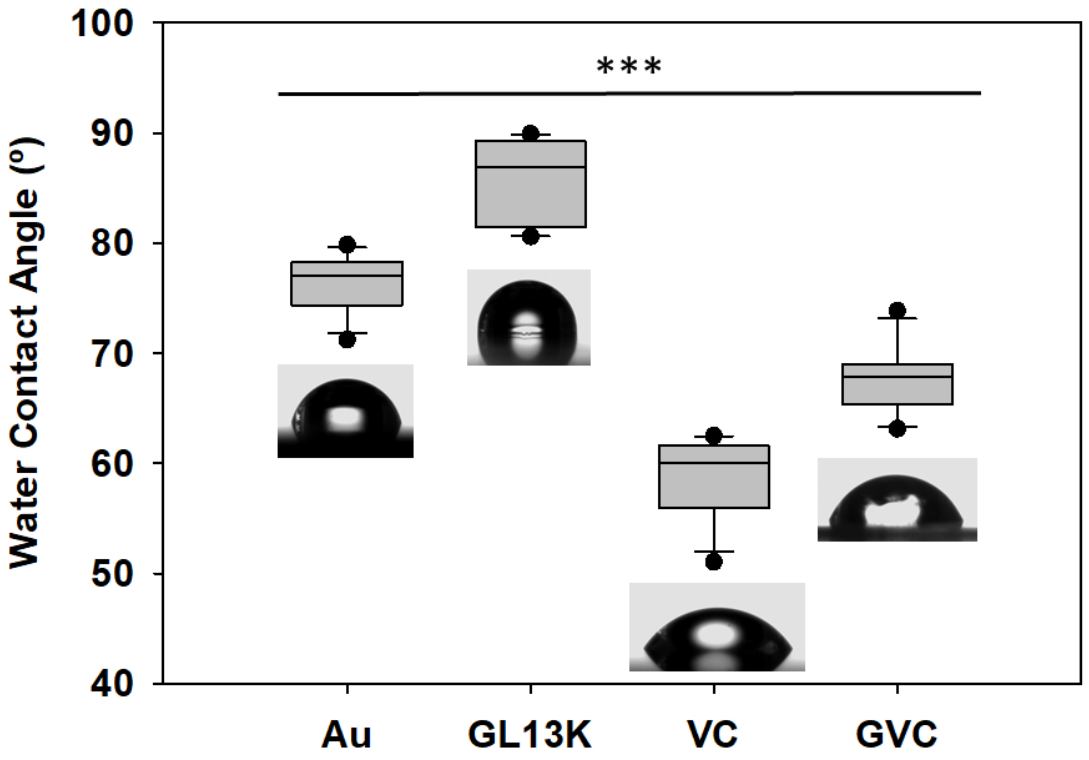

Figure 2. Static water contact angle of the gold surfaces when the AMP/ELRs are covalently attached. Depending on the physicochemical properties of the molecules, the wettability of the surfaces changes significantly (***$p < 0.001$). At least 10 different measurements for each surface are represented in the box diagram. Error bars represent standard deviation values.

The elemental composition was quantified by XPS. The atomic percentages of the coatings are shown in Table S3. A variation in the percentage of signature atoms with respect to the control (Au surfaces) could be detected. Thus, nitrogen (N 1s, characteristic peak for proteins) content increased from an initial 0% up to 12–14% for GL13K, VC and GVC coated surfaces. Furthermore, the decrease in Au content for these three surfaces indicated the deposition effectiveness of the AMP/ELR. Moreover, when gold surfaces were modified with thiols, the energy for the Au 4f peak shifted, [63] thus indicating covalent attachment to the surface (see Figure S3).

Finally, the thickness and the area density of the SAMs were estimated quantitatively using the QCM-D technique.

First, the viscous penetration depth (δ) corresponding to ultrapure water, the solvent used, was estimated [64]. The decay rate of the oscillating wave with the distance from the sensor surface is indicated by (Eq. 1).

$$\delta = \sqrt{\frac{2\eta}{\rho\omega}} \qquad \text{(Eq. 1)}$$

Where η and ρ are the viscosity and density of the solution employed for the measurement, respectively, and ω is the oscillation frequency. For ultrapure water (η = 0.93 mPa·s and ρ = 0.998 g/cm^3), δ is approximately 140 nm at 15 MHz (third overtone, n = 3).

QCM-D measurements were performed at 23°C. The simultaneously measured shifts in frequency (normalized to the corresponding overtone, n), $\Delta f_n/n$ (Figure 3A), and energy dissipation, ΔD_n (Figure 3B), obtained at n = 5 (25 MHz) are plotted as a function of time. Although measurements were carried out up to the 13th overtone (65 MHz), only the fifth harmonic is shown in Figure 3 for clarity. Frequency and dissipation changes corresponding to the fifth, seventh and ninth overtones are reported in the Supporting Information (Figure S4).

Three events can be identified in the transient evolution: (i) flow of ultrapure water to establish the baseline, (ii) flow of the AMP/ELR solution, (iii) rinsing with ultrapure water. when frequency changes are considered (Figure 3A), at the beginning of the deposition stage, the slope of the frequency change was slightly higher for GVC than for VC deposition. In addition, the frequency stabilized for GL13K and VC during the deposition stage, whereas a roughly linear decrease of frequency with time was observed

for GVC. Specifically, at the end of the deposition stage, the frequency changes observed were −3.6, −12, and −18 Hz, for GL13K, VC, and GVC, respectively. During the final rinsing stage, a slight increase in frequency of between +1 and +2 Hz was observed for all the biomaterials, thus indicating a minor desorption of molecules.

As far as dissipation is concerned (Figure 3B), a plateau was reached for GL13K and VC solutions during the deposition stage, whereas a slight slope in the dissipation was observed for GVC, similar to the frequency evolution. The rinsing stage resulted in a decrease in dissipation, and at the end of the rinsing stage a dissipation of close to zero was observed for the GL13K peptide, whereas values of around 1×10^{-6} and 3×10^{-6} were found for the ELRs GVC and VC, respectively.

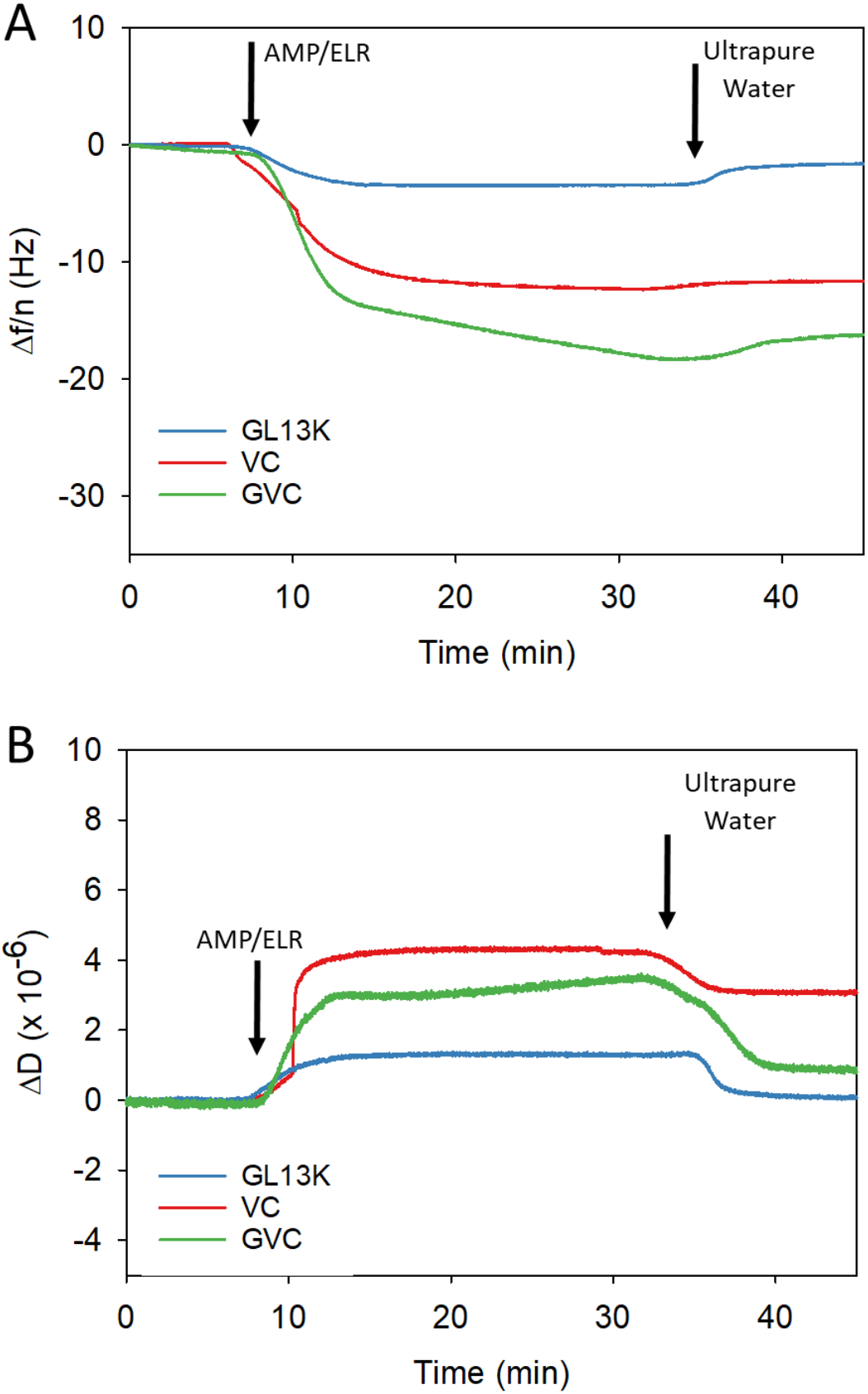

Figure 3. (A) Normalized frequency and (B) energy dissipation shifts measured at 23 °C at the fifth (n = 5) overtone for GL13K, VC, and GVC. Three events are distinguished: first, an ultrapure water stabilization flow for 2 min; second, the AMP/ELR solutions were exposed for 25 min; and finally, a stage of rinsing with ultrapure water for 20 min.

As a whole, the time evolution of the frequency change is similar for both ELRs (VC and

GVC) and clearly differs from that for the peptide. The difference in molecular weights between these molecules may explain this behavior.

Because overtones are split in terms of both frequency and dissipation changes (Figure S4A), the simple Sauerbrey model is not valid, therefore a viscoelastic model that enables thin film areas and masses to be calculated from multiple harmonics is required. In this case, a Voigt viscoelastic model based on a single layer was used. [65,66] In this model, the adsorbed film is represented by a lateral homogeneous film with uniform thickness and density which, in our case, was estimated at 1.1 g/cm^3 (corresponding to a hydrated protein). [67] The thickness of the adsorbed thin film was subsequently calculated using the QCM-D raw data.

At the end of the experiment, the Voigt model provides the thickness and the corresponding area density that characterize the stabilized thin film. The values for GL13K, VC, and GVC recombinamers are summarized in Table 2.

Table 2. Thickness and Area Density of the AMP/ELRs Immobilized on the Gold Surfaces at the End of the Rinsing Stage, As Calculated Using the Voigt Model and the Raw QCM-D Experimental Data.

	GL13K	**VC**	**GVC**
Thickness (nm)	1.7±0.2	14.4±2.8	15.5±1.4
Area density (ng/cm^2)	155±63.6	1575±318.2	1675±106.1

Similar thicknesses were obtained for VC and GVC coatings, with these values being clearly higher than the thickness for GL13K. This may be attributed to the molecular

weight differences between the AMP and the ELRs. These results are consistent with the elemental quantification obtained by XPS.

Biofunctional Evaluation of Recombinant SAMs

Antibiofilm Activity of Recombinant SAMs

SEM images (Figures 4 and 5) of the biofilms revealed that, after overnight incubation, the pristine gold surfaces (Au) were completely covered by multiple layers of bacteria nd

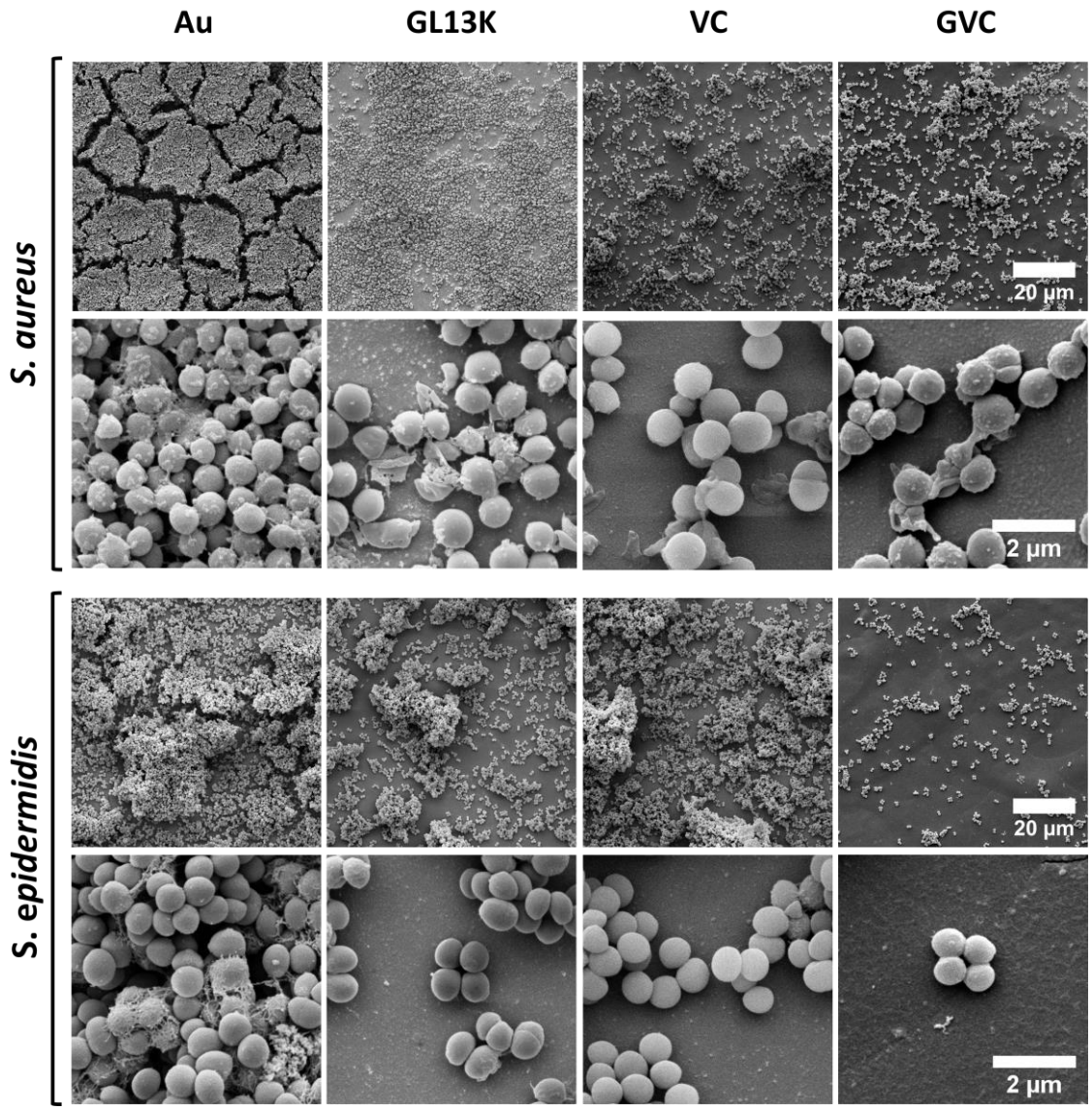

Figure 4. Representative SEM micrographs of the biofilms formed onto the different coatings and control Au surfaces after 24 h incubation. General view (1st and 3rd rows) and close-up (2nd and 4th rows) images of the *S. aureus* (1st and 2nd rows) and *S. epidermidis* (3rd and 4th rows) biofilms. Comparing to control gold surfaces (Au), all coatings had an antibiofilm effect that prevented the formation of a mature biofilm for both staphylococcal strains. S. aureus bacteria on GL13K and GVC coatings had disrupted walls and/or distorted shapes.

extracellular matrix for both staphylococcal strains. All SAMs had antibiofilm effects, even in the case of the recombinamer control (VC) coating. Indeed, all three coatings prevented the formation of a mature biofilm of both staphylococcal strains, but with clear differences between the two strains. Thus, the antibiofilm activity of the nanocoatings seemed to be stronger against *S. aureus* than against *S. epidermidis*, except for GVC, as this coating showed a high potency of biofilm inhibition against both strains.

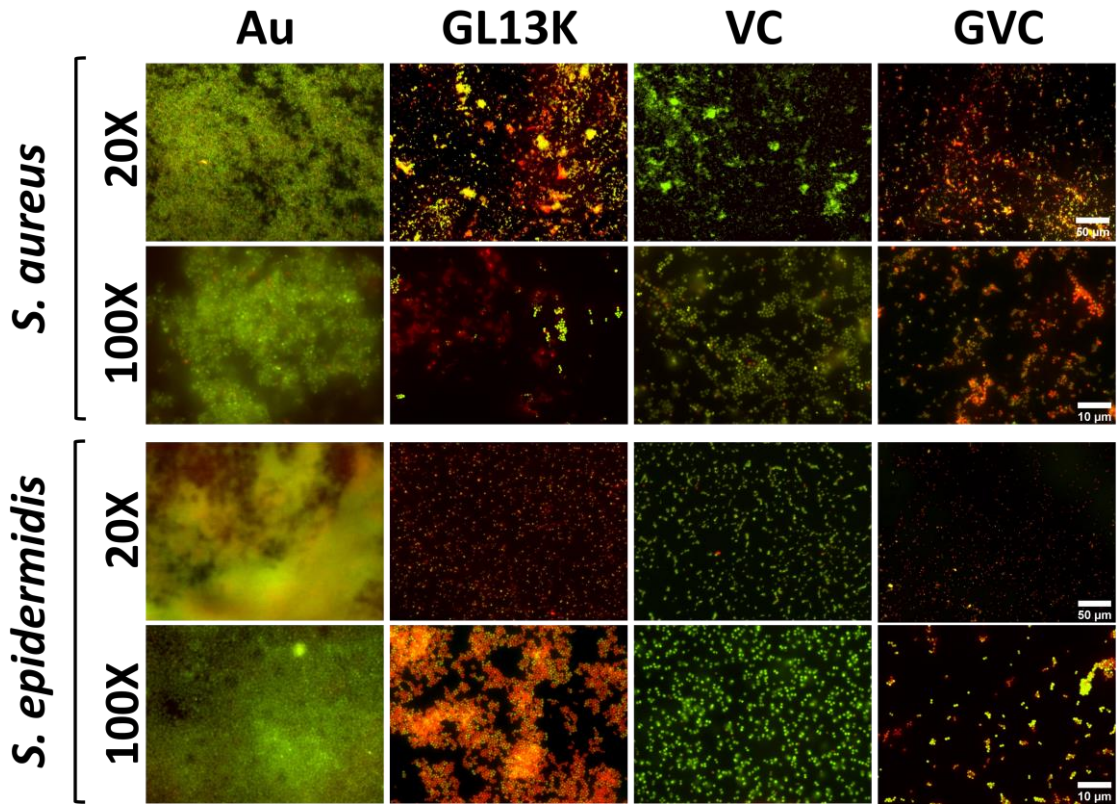

Figure 5. Live/Dead staining biofilms after 24 h of incubation on the surfaces. Green cells correspond to live cells, whereas red cells correspond with death or damaged cells. Gold surfaces were found completely covered by a multilayer biofilm, whereas all the coatings prevent the biofilm development. Bactericidal activity against *S. aureus* and *S. epidermidis* bacteria were also found on those coatings that show the GL13K peptide (GL13K and GVC).

Fluorescence microscopy with Live/Dead (L/D) staining (Figure 5) confirmed that the VC coating had a low-fouling effect that hampered biofilm formation in comparison to mature biofilms grown on control pristine gold surfaces. However, the VC coatings did not exhibit bactericidal activity (Figure 5, third column). Elastin-like coatings have previously been shown to exhibit antifouling properties,[42–44] which here could lead to low

adhesion of staphylococci and, consequently, low biofilm formation. In addition, we verified that the presence of the GL13K peptide on the surfaces (GL13K and GVC SAMs) prevented development of a mature biofilm and also exhibited bactericidal activity against the bacteria that reached the surface, thus minimizing bacterial colonization. It is worth noting that the bactericidal effects of the SAMs with GL13K peptides resulted in shape distortion and bacterial disruption of *S. aureus* (Figure 4, second row), as described previously for oral Gram (+) bacteria, such as *Streptococcus gordonii*. [22]

Quantification of antibiofilm activity supported these conclusions (Figure 6). Thus, the CV assay showed a significant decrease in the total remaining biomass when the staphylococci were incubated on the SAMs when compared with control gold surfaces. Similarly, ATP quantification confirmed the antibiofilm and bactericidal effect of the coatings containing the GL13K peptide (GL13K and GVC). On these SAMs, the metabolic activity of the bacteria was significantly lower than that on control Au surfaces and VC coatings (Figure 6).

t is important to note that a divergence between the CV and ATP values for the control ELR (VC) was found. Thus, the bacterial biomass was significantly lower than for the control naked Au surfaces, whereas ATP values did not differ markedly. The minor differences observed in the metabolic activity between the biofilms formed on Au and VC surfaces may be due to biofilm heterogeneity. Despite the inhibition of mature biofilm development (see CV results and SEM images), VC coatings do not exhibit bactericidal activity (L/D images), thus meaning that the bacteria remaining are metabolically active. However, within a mature biofilm (gold surfaces), bacterial cells show physiological heterogeneity.[68] Bacterial immobilization on a surface triggers their adaptation to new environmental conditions, thus resulting in diverse bacterial subcommunities. In a mature biofilm, nutrients, oxygen and toxic metabolite concentration gradients differ depending

on the spatial situation.[69] Thus, the bacteria that remain within the biofilm are in an averaged lower metabolic state when compared with recently attached or superficial bacteria. Thus, the combination of different techniques is of relevance in this case to allow a more comprehensive set of antimicrobial properties to be assessed, thereby enabling a better description of the biofunctional activity of new coatings developed for preventing infection in biomedical applications.

Combining Low-Fouling ELR with AMP: Synergistic Convergence of Antimicrobial Properties

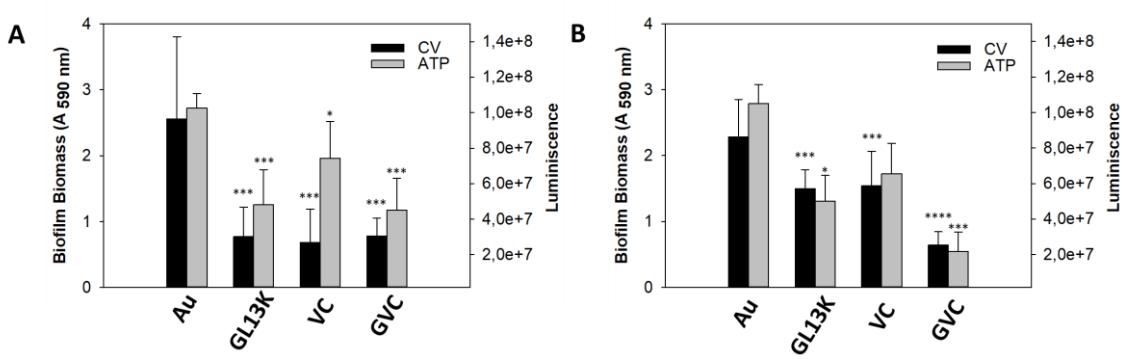

Figure 6. Antibiofilm activity of the coatings against (A) S. aureus 25923 and (B) S. epidermidis 35984 biofilms after 24 h of incubation in TSB medium with extra glucose (1%). Biofilm total biomass and ATP quantification demonstrated the strong and significant (**** $p < 0.0001$, *** $p < 0.001$, * $p < 0.05$ comparing with control Au surfaces) antibiofilm activity of the coating GVC. Error bars are the standard deviation of at least four samples in each group.

Striking differences were found between the antimicrobial effects of the coatings on each of the two staphylococcal strains. Thus, *S. aureus* biofilms were more sensitive to the antibiofilm activity of the SAMs than *S. epidermidis* biofilms. In addition, the CV values for *S. aureus* biofilms were 3-fold lower for all three SAMs than for control gold surfaces (Figure 6A). However, the metabolic activity of *S. aureus* bacteria that remained onto the surfaces was significantly lower on those SAMs that showed the GL13K peptide (GL13K

and GVC) compared with the VC coating ($p < 0.05$), thus demonstrating that the presence of the GL13K peptide onto the surfaces also provided a bactericidal effect.

Interestingly, *S. epidermidis* biofilms seemed to be more resistant to the antibiofilm properties of only GL13K and the VC coated surfaces. Thus, although *S. epidermis* biofilm inhibition by these two coatings was also noticeable, it was less pronounced (Figure 4, third and fourth rows and Figure 6B) than against *S. aureus* biofilms (Figure 4, first and second rows and Figure 6A). However, the surfaces coated with GVC, which contains both the ELR and the AMP, was highly effective against both strains. Despite the fact that similar activity against *S. aureus* biofilms to that for GL13K was observed for the chimeric SAM (GVC), the low-fouling activity of the ELR and the antibiofilm and bactericidal activities of the AMP (GL13K peptide) converge in a synergistic manner, thereby increasing the antibiofilm effect against the otherwise resistant *S. epidermidis* biofilms.

These differences in the antibiofilm activity against both staphylococcal biofilms could be a consequence of the diverse nature of both biofilms. Biofilm integrity is sustained by different biomolecules [70] (mainly extracellular DNA for *S. aureus* and poly-N-acetylglucosamine for *S. epidermidis*) and adherence proteins also differ widely. [71]

The molecular mechanisms describing the interactions of immobilized AMPs are still uncertain. Recent studies have proposed that the killing mechanism for cationic AMPs immobilized on surfaces may be mediated simply by electrostatic interactions between the AMP and the bacterial surface, [72] with no cell membrane interactions, as reported for AMPs in solution. [73] hus, in light of our results, we suggest that the conjugation of AMPs with ELRs enables the formation of highly potent antibiofilm coatings as the ELR provides a low-fouling scaffold for the bactericidal AMP, thus meaning that the

recombinant SAMs synergistically combine antibiofilm activity and a decrease in bacterial attachment, consistent with recent studies on chemical antiadherent coatings with AMPs. [26] These SAMs may also result in effective antimicrobial electrostatic interactions, thereby increasing the antibiofilm effect of the GL13K peptides.

Selective Toxicity against Bacteria

Finally, the cytocompatibility of the surfaces was assessed to demonstrate that the toxic effect is selective for bacteria and does not affect the proliferation of human cells. thus, a metabolic assay with AlamarBlue (Figure 7) proved that the recombinant coatings were not cytotoxic for human fibroblasts for in vitro culture periods of up to 7 days.

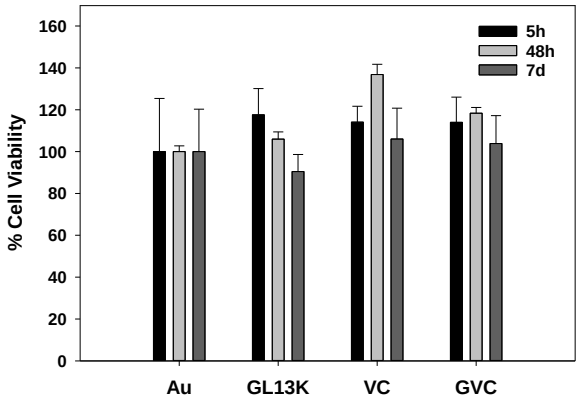

Figure 7. Cytocompatibility of GL13K, VC and GVC coatings after 5, 48 h and 1 week of incubation with Human Foreskin Fibroblasts using the AlamarBlue assay. Results are expressed as % cell viability with respect to the control. Bars represent mean ± standard deviation. No significant differences between coatings were found deviation. No significant differences between coatings were found.

Conclusions

Using a multimodular design for ELRs, we have demonstrated that the conjugation of an AMP to a low-fouling ELR can be used to produce SAMs with strong and synergistic antibiofilm potency against staphylococcal strains. This biomolecular-based biomaterial was produced using recombinant technologies and sheds light on the potential of

conjugating AMPs to recombinant polymers to form new antibiofilm agents for nanocoatings with excellent versatility, technical feasibility, and multifunctional properties. In addition, the easy and relatively cheap production and purification procedures for these recombinant compounds, which exploits the thermal sensitivity of their ELR part, facilitates scale-up of their production and potential widespread use.

Supporting Information

Data regarding the characterization of the ELRs (SDS-PAGE, MALDI-TOF, and HPLC) and from the physical characterization of the surfaces (XPS spectra and QCM-D measurements) are provided in the "Supporting Information for publication" file.

Acknowledgements

The authors acknowledge Dr. Arturo Ibañez and Dr. Javier Arias-Vallejo, Bioforge group, University of Valladolid, for technical assistance during the optimization of the bioproduction; Tatjana Flora, Bioforge group, University of Valladolid for technical assistance with cytocompatibility tests. The authors are grateful for the funding from the European Commission (NMP-2014-646075), Minister of Science of the Spanish Government (PCIN-2015-010, MAT2015-68901-R, MAT2016-78903-R), Junta de Castilla y León (VA317P18) and Centro en Red de Medicina Regenerativa y Terapia Celular de Castilla y León.

References

(1) Dickinson, G. M.; Bisno, A. L. Infections Associated with Indwelling Devices: Infections Related to Extravascular Devices. *Antimicrob. Agents Chemother.* **1989**, *33* (5), 602–607, DOI: 10.1128/aac.33.5.602.

(2) Donlan, R. M. Biofilms on Central Venous Catheters: Is Eradication Possible? *Curr. Top. Microbiol. Immunol.* **2008**, *322*, 133–161, DOI: 10.1007/978-3-540-75418-3_7.

(3) Boucher, H. W.; Talbot, G. H.; Bradley, J. S.; Edwards, J. E.; Gilbert, D.; Rice, L. B.; Scheld, M.; Spellberg, B.; Bartlett, J. Bad Bugs, No Drugs: No ESKAPE! An Update from the Infectious

Diseases Society of America. *Clin. Infect. Dis.* **2009**, *48* (1), 1–12, DOI: 10.1086/595011.

(4) Otto, M. Staphylococcal Biofilms. *Current Topics in Microbiology and Immunology*. Springer, Berlin, Heidelberg 2008, pp 207–228, DOI: 10.1007/978-3-540-75418-3_10.

(5) Weiner, L. M.; Webb, A. K.; Limbago, B.; Dudeck, M. A.; Patel, J.; Kallen, A. J.; Edwards, J. R.; Sievert, D. M. Antimicrobial-Resistant Pathogens Associated With Healthcare-Associated Infections: Summary of Data Reported to the National Healthcare Safety Network at the Centers for Disease Control and Prevention, 2011–2014. *Infect. Control Hosp. Epidemiol.* **2016**, *37* (11), 1288–1301, DOI: 10.1017/ice.2016.174.

(6) Pham, V. T. H.; Bhadra, C. M.; Truong, V. K.; Crawford, R. J.; Ivanova, E. P. Designing Antibacterial Surfaces for Biomedical Implants. In *Antibacterial Surfaces*; Springer International Publishing: Cham, 2015; pp 89–111, DOI: 10.1007/978-3-319-18594-1_6.

(7) Cloutier, M.; Mantovani, D.; Rosei, F. Antibacterial Coatings: Challenges, Perspectives, and Opportunities. *Trends Biotechnol.* **2015**, *33* (11), 637–652, DOI: 10.1016/J.TIBTECH.2015.09.002.

(8) Darouiche, R. O.; Raad, I. I.; Heard, S. O.; Thornby, J. I.; Wenker, O. C.; Gabrielli, A.; Berg, J.; Khardori, N.; Hanna, H.; Hachem, R.; et al. A Comparison of Two Antimicrobial-Impregnated Central Venous Catheters. *N. Engl. J. Med.* **1999**, *340* (1), 1–8, DOI: 10.1056/NEJM199901073400101.

(9) Kuehl, R.; Brunetto, P. S.; Woischnig, A.-K.; Varisco, M.; Rajacic, Z.; Vosbeck, J.; Terracciano, L.; Fromm, K. M.; Khanna, N. Preventing Implant-Associated Infections by Silver Coating. *Antimicrob. Agents Chemother.* **2016**, *60* (4), 2467–2475, DOI: 10.1128/AAC.02934-15.

(10) McGuffie, M. J.; Hong, J.; Bahng, J. H.; Glynos, E.; Green, P. F.; Kotov, N. A.; Younger, J. G.; VanEpps, J. S. Zinc Oxide Nanoparticle Suspensions and Layer-by-Layer Coatings Inhibit Staphylococcal Growth. *Nanomedicine Nanotechnology, Biol. Med.* **2016**, *12* (1), 33–42, DOI: 10.1016/J.NANO.2015.10.002.

(11) Jain, A.; Duvvuri, L. S.; Farah, S.; Beyth, N.; Domb, A. J.; Khan, W. Antimicrobial Polymers. *Adv. Healthc. Mater.* **2014**, *3* (12), 1969–1985, DOI: 10.1002/adhm.201400418.

(12) Stewart, P. S.; William Costerton, J. Antibiotic Resistance of Bacteria in Biofilms. *Lancet* **2001**, *358* (9276), 135–138, DOI: 10.1016/S0140-6736(01)05321-1.

(13) Politano, A. D.; Campbell, K. T.; Rosenberger, L. H.; Sawyer, R. G. Use of Silver in the Prevention and Treatment of Infections: Silver Review. *Surg. Infect. (Larchmt).* **2013**, *14* (1), 8–20, DOI: 10.1089/sur.2011.097.

(14) Hanley, C.; Layne, J.; Punnoose, A.; Reddy, K. M.; Coombs, I.; Coombs, A.; Feris, K.; Wingett, D. Preferential Killing of Cancer Cells and Activated Human T Cells Using ZnO Nanoparticles. *Nanotechnology* **2008**, *19* (29), 295103, DOI: 10.1088/0957-4484/19/29/295103.

(15) Timofeeva, L.; Kleshcheva, N. Antimicrobial Polymers: Mechanism of Action, Factors of Activity, and Applications. *Applied Microbiology and Biotechnology*. 2011, pp 475–492, DOI: 10.1007/s00253-010-2920-9.

(16) Guilhelmelli, F.; Vilela, N.; Albuquerque, P.; Derengowski, L. da S.; Silva-Pereira, I.; Kyaw, C. M. Antibiotic Development Challenges: The Various Mechanisms of Action of Antimicrobial Peptides and of Bacterial Resistance. *Frontiers in Microbiology*. Frontiers December 9, 2013, p 353, DOI: 10.3389/fmicb.2013.00353.

(17) Ye, Zhou; Zhu, Xiao; Acosta, Sergio; Aparicio, C. Self-Assembly Dynamics and Antimicrobial Activity of All Land D-Amino Acid Enantiomers of a Designer Peptide. *Nanoscale* **2019**, *11*, 266–275, DOI: 10.1039/C8NR07334A.

(18) Hancock, R. E. W.; Sahl, H. G. Antimicrobial and Host-Defense Peptides as New Anti-Infective Therapeutic Strategies. *Nature Biotechnology*. 2006, pp 1551–1557, DOI: 10.1038/nbt1267.

(19) Townsend, L.; Williams, R. L.; Anuforom, O.; Berwick, M. R.; Halstead, F.; Hughes, E.; Stamboulis, A.; Oppenheim, B.; Gough, J.; Grover, L.; et al. Antimicrobial Peptide Coatings for

Hydroxyapatite: Electrostatic and Covalent Attachment of Antimicrobial Peptides to Surfaces. *J. R. Soc. Interface* **2017**, *14* (126), DOI: 10.1098/rsif.2016.0657.

(20) Holmberg, K. V.; Abdolhosseini, M.; Li, Y.; Chen, X.; Gorr, S.-U.; Aparicio, C. Bio-Inspired Stable Antimicrobial Peptide Coatings for Dental Applications. *Acta Biomater.* **2013**, *9* (9), 8224–8231, DOI: 10.1016/j.actbio.2013.06.017.

(21) Yu, K.; Lo, J. C. Y.; Yan, M.; Yang, X.; Brooks, D. E.; Hancock, R. E. W.; Lange, D.; Kizhakkedathu, J. N. Anti-Adhesive Antimicrobial Peptide Coating Prevents Catheter Associated Infection in a Mouse Urinary Infection Model. *Biomaterials* **2017**, *116*, 69–81, DOI: 10.1016/j.biomaterials.2016.11.047.

(22) Chen, X.; Hirt, H.; Li, Y.; Gorr, S. U.; Aparicio, C. Antimicrobial GL13K Peptide Coatings Killed and Ruptured the Wall of Streptococcus Gordonii and Prevented Formation and Growth of Biofilms. *PLoS One* **2014**, *9* (11), e111579, DOI: 10.1371/journal.pone.0111579.

(23) Chen, R.; Cole, N.; Willcox, M. D. P.; Park, J.; Rasul, R.; Carter, E.; Kumar, N. Synthesis, Characterization and *in Vitro* Activity of a Surface-Attached Antimicrobial Cationic Peptide. *Biofouling* **2009**, *25* (6), 517–524, DOI: 10.1080/08927010902954207.

(24) Kumar, P.; Takayesu, A.; Abbasi, U.; Kalathottukaren, M. T.; Abbina, S.; Kizhakkedathu, J. N.; Straus, S. K. Antimicrobial Peptide–Polymer Conjugates with High Activity: Influence of Polymer Molecular Weight and Peptide Sequence on Antimicrobial Activity, Proteolysis, and Biocompatibility. *ACS Appl. Mater. Interfaces* **2017**, *9* (43), 37575–37586, DOI: 10.1021/acsami.7b09471.

(25) Gao, Q.; Yu, M.; Su, Y.; Xie, M.; Zhao, X.; Li, P.; Ma, P. X. Rationally Designed Dual Functional Block Copolymers for Bottlebrush-like Coatings: In Vitro and in Vivo Antimicrobial, Antibiofilm, and Antifouling Properties. *Acta Biomater.* **2017**, *51*, 112–124, DOI: 10.1016/J.ACTBIO.2017.01.061.

(26) Shtreimer Kandiyote, N.; Avisdris, T.; Arnusch, C. J.; Kasher, R. Grafted Polymer Coatings Enhance Fouling Inhibition by an Antimicrobial Peptide on Reverse Osmosis Membranes. *Langmuir* **2019**, *35* (5), 1935–1943, DOI: 10.1021/acs.langmuir.8b03851.

(27) Gabriel, M.; Nazmi, K.; Veerman, E. C.; Amerongen, A. V. N.; Zentner, A. Preparation of LL-37-Grafted Titanium Surfaces with Bactericidal Activity. *Bioconjug. Chem.* **2006**, *17* (2), 548–550, DOI: 10.1021/bc050091v.

(28) Glinel, K.; Jonas, A. M.; Jouenne, T.; Leprince, J.; Galas, L.; Huck, W. T. S. Antibacterial and Antifouling Polymer Brushes Incorporating Antimicrobial Peptide. *Bioconjug. Chem.* **2009**, *20* (1), 71–77, DOI: 10.1021/bc800280u.

(29) Shtreimer Kandiyote, N.; Mohanraj, G.; Mao, C.; Kasher, R.; Arnusch, C. J. Synergy on Surfaces: Anti-Biofouling Interfaces Using Surface-Attached Antimicrobial Peptides PGLa and Magainin-2. *Langmuir* **2018**, *34* (37), 11147–11155, DOI: 10.1021/acs.langmuir.8b01617.

(30) Muszanska, A. K.; Rochford, E. T. J.; Gruszka, A.; Bastian, A. A.; Busscher, H. J.; Norde, W.; van der Mei, H. C.; Herrmann, A. Antiadhesive Polymer Brush Coating Functionalized with Antimicrobial and RGD Peptides to Reduce Biofilm Formation and Enhance Tissue Integration. *Biomacromolecules* **2014**, *15* (6), 2019–2026, DOI: 10.1021/bm500168s.

(31) Atefyekta, S.; Pihl, M.; Lindsay, C.; Heilshorn, S. C.; Andersson, M. Antibiofilm Elastin-like Polypeptide Coatings: Functionality, Stability, and Selectivity. *Acta Biomater.* **2019**, *83*, 245–256, DOI: 10.1016/j.actbio.2018.10.039.

(32) Wadhwani, P.; Heidenreich, N.; Podeyn, B.; Bürck, J.; Ulrich, A. S. Antibiotic Gold: Tethering of Antimicrobial Peptides to Gold Nanoparticles Maintains Conformational Flexibility of Peptides and Improves Trypsin Susceptibility. *Biomater. Sci.* **2017**, *5* (4), 817–827, DOI: 10.1039/C7BM00069C.

(33) Andersson, L.; Blomberg, L.; Flegel, M.; Lepsa, L.; Nilsson, B.; Verlander, M. Large-Scale Synthesis of Peptides. *Biopolymers* **2000**, *55* (3), 227–250, DOI: 10.1002/1097-0282(2000)55:3<227::AID-BIP50>3.0.CO;2-7.

(34) Krahulec, J.; Hyršová, M.; Pepeliaev, S.; Jílková, J.; Černý, Z.; Machálková, J. High Level Expression and Purification of Antimicrobial Human Cathelicidin LL-37 in Escherichia Coli. *Appl. Microbiol. Biotechnol.* **2010**, *88* (1), 167–175, DOI: 10.1007/s00253-010-2736-7.

(35) Bommarius, B.; Jenssen, H.; Elliott, M.; Kindrachuk, J.; Pasupuleti, M.; Gieren, H.; Jaeger, K.-E.; Hancock, R. E. W.; Kalman, D. Cost-Effective Expression and Purification of Antimicrobial and Host Defense Peptides in Escherichia Coli. *Peptides* **2010**, *31* (11), 1957–1965, DOI: 10.1016/J.PEPTIDES.2010.08.008.

(36) Srinivasulu, B.; Syvitski, R.; Seo, J. K.; Mattatall, N. R.; Knickle, L. C.; Douglas, S. E. Expression, Purification and Structural Characterization of Recombinant Hepcidin, an Antimicrobial Peptide Identified in Japanese Flounder, Paralichthys Olivaceus. *Protein Expr. Purif.* **2008**, *61* (1), 36–44, DOI: 10.1016/j.pep.2008.05.012.

(37) Bommarius, B.; Jenssen, H.; Elliott, M.; Kindrachuk, J.; Pasupuleti, M.; Gieren, H.; Jaeger, K.-E.; Hancock, R. E. W.; Kalman, D. Cost-Effective Expression and Purification of Antimicrobial and Host Defense Peptides in Escherichia Coli. *Peptides* **2010**, *31* (11), 1957–1965, DOI: 10.1016/j.peptides.2010.08.008.

(38) Wu, W.-Y.; Mee, C.; Califano, F.; Banki, R.; Wood, D. W. Recombinant Protein Purification by Self-Cleaving Aggregation Tag. *Nat. Protoc.* **2006**, *1* (5), 2257–2262, DOI: 10.1038/nprot.2006.314.

(39) Hassouneh, W.; Christensen, T.; Chilkoti, A. Elastin-like Polypeptides as a Purification Tag for Recombinant Proteins. *Curr. Protoc. Protein Sci.* **2010**, No. SUPPL. 61, 1–20, DOI: 10.1002/0471140864.ps0611s61.

(40) Da Costa, A.; Machado, R.; Ribeiro, A.; Collins, T.; Thiagarajan, V.; Neves-Petersen, M. T.; Rodriguez-Cabello, J. C.; Gomes, A. C.; Casal, M. Development of Elastin-like Recombinamer Films with Antimicrobial Activity. *Biomacromolecules* **2015**, *16* (2), DOI: 10.1021/bm5016706.

(41) da Costa, A.; Pereira, A. M.; Gomes, A. C.; Rodriguez-Cabello, J. C.; Casal, M.; Machado, R. Production of Bioactive Hepcidin by Recombinant DNA Tagging with an Elastin-like Recombinamer. *N. Biotechnol.* **2018**, *46*, 45–53, DOI: 10.1016/J.NBT.2018.07.001.

(42) Urry, D. W.; Parker, T. M.; Reid, M. C.; Gowda, D. C. Biocompatibility of the Bioelastic Materials, Poly(GVGVP) and Its γ-Irradiation Cross-Linked Matrix: Summary of Generic Biological Test Results. *J. Bioact. Compat. Polym.* **1991**, *6* (3), 263–282, DOI: 10.1177/088391159100600306.

(43) Pierna, M.; Santos, M.; Arias, F. J.; Alonso, M.; Rodríguez-Cabello, J. C. Efficient Cell and Cell-Sheet Harvesting Based on Smart Surfaces Coated with a Multifunctional and Self-Organizing Elastin-Like Recombinamer. *Biomacromolecules* **2013**, *14* (6), 1893–1903, DOI: 10.1021/bm400268v.

(44) Salvagni, E.; Berguig, G.; Engel, E.; Rodriguez-Cabello, J. C.; Coullerez, G.; Textor, M.; Planell, J. A.; Gil, F. J.; Aparicio, C. A Bioactive Elastin-like Recombinamer Reduces Unspecific Protein Adsorption and Enhances Cell Response on Titanium Surfaces. *Colloids Surfaces B Biointerfaces* **2014**, *114*, 225–233, DOI: 10.1016/j.colsurfb.2013.10.008.

(45) Abdolhosseini, M.; Nandula, S. R.; Song, J.; Hirt, H.; Gorr, S.-U. Lysine Substitutions Convert a Bacterial-Agglutinating Peptide into a Bactericidal Peptide That Retains Anti-Lipopolysaccharide Activity and Low Hemolytic Activity. *Peptides* **2012**, *35* (2), 231–238, DOI: 10.1016/j.peptides.2012.03.017.

(46) Chen, R.; Willcox, M. D. P.; Cole, N.; Ho, K. K. K.; Rasul, R.; Denman, J. A.; Kumar, N. Characterization of Chemoselective Surface Attachment of the Cationic Peptide Melimine and Its Effects on Antimicrobial Activity. *Acta Biomater.* **2012**, *8* (12), 4371–4379, DOI: 10.1016/J.ACTBIO.2012.07.029.

(47) Costa, F.; Gomes, P.; Martins, M. C. L. Antimicrobial Peptides (AMP) Biomaterial Coatings for Tissue Repair. In *Peptides and Proteins as Biomaterials for Tissue Regeneration and Repair*; Woodhead Publishing, 2017; pp 329–345, DOI: 10.1016/B978-0-08-100803-4.00013-9.

(48) Xiao, S. J.; Textor, M.; Spencer, N. D.; Wieland, M.; Keller, B.; Sigrist, H. Immobilization of the

Cell-Adhesive Peptide Arg-Gly-Asp-Cys (RGDC) on Titanium Surfaces by Covalent Chemical Attachment. In *Journal of Materials Science: Materials in Medicine*; Kluwer Academic Publishers, 1997; Vol. 8, pp 867–872, DOI: 10.1023/A:1018501804943.

(49) Lateef, S. S.; Boateng, S.; Hartman, T. J.; Crot, C. A.; Russell, B.; Hanley, L. GRGDSP Peptide-Bound Silicone Membranes Withstand Mechanical Flexing in Vitro and Display Enhanced Fibroblast Adhesion. *Biomaterials* **2002**, *23* (15), 3159–3168, DOI: 10.1016/S0142-9612(02)00062-5.

(50) Zhang, L.; Vilà, N.; Klein, T.; Kohring, G.-W.; Mazurenko, I.; Walcarius, A.; Etienne, M. Immobilization of Cysteine-Tagged Proteins on Electrode Surfaces by Thiol−Ene Click Chemistry. **2016**, DOI: 10.1021/acsami.6b02364.

(51) Sabourin, M.; Tuzon, C. T.; Fisher, T. S.; Zakian, V. A. A Flexible Protein Linker Improves the Function of Epitope-Tagged Proteins in Saccharomyces Cerevisiae. *Yeast* **2007**, *24* (1), 39–45, DOI: 10.1002/yea.1431.

(52) Etayash, H.; Norman, L.; Thundat, T.; Stiles, M.; Kaur, K. Surface-Conjugated Antimicrobial Peptide Leucocin A Displays High Binding to Pathogenic Gram-Positive Bacteria. *ACS Appl. Mater. Interfaces* **2014**, *6* (2), 1131–1138, DOI: 10.1021/am404729c.

(53) Maloy, W. L.; Kari, U. P. Structure-Activity Studies on Magainins and Other Host Defense Peptides. *Biopolymers* **1995**, *37* (2), 105–122, DOI: 10.1002/bip.360370206.

(54) Meyer, D. E.; Chilkoti, A. Genetically Encoded Synthesis of Protein-Based Polymers with Precisely Specified Molecular Weight and Sequence by Recursive Directional Ligation: Examples from the the Elastin-like Polypeptide System. *Biomacromolecules* **2002**, *3* (2), 357–367, DOI: 10.1021/bm015630n.

(55) Rodríguez-Cabello, J. C.; Girotti, A.; Ribeiro, A.; Arias, F. J. Synthesis of Genetically Engineered Protein Polymers (Recombinamers) as an Example of Advanced Self-Assembled Smart Materials. *Methods Mol. Biol.* **2012**, *811*, 17–38, DOI: 10.1007/978-1-61779-388-2_2.

(56) Xue, Y.; Li, X.; Li, H.; Zhang, W. Quantifying Thiol–Gold Interactions towards the Efficient Strength Control. *Nat. Commun.* **2014**, *5* (1), 4348, DOI: 10.1038/ncomms5348.

(57) Rodahl, M.; Höök, F.; Fredriksson, C.; Keller, C. A.; Krozer, A.; Brzezinski, P.; Voinova, M.; Kasemo, B. Simultaneous Frequency and Dissipation Factor QCM Measurements of Biomolecular Adsorption and Cell Adhesion. *Faraday Discuss.* **1997**, *107* (0), 229–246, DOI: 10.1039/a703137h.

(58) Rodahl, M.; Kasemo, B. On the Measurement of Thin Liquid Overlayers with the Quartz-Crystal Microbalance. *Sensors Actuators A Phys.* **1996**, *54* (1–3), 448–456, DOI: 10.1016/S0924-4247(97)80002-7.

(59) Dantzig, G. A History of Scientific Computing. *Computing* **1990**, 88–105, DOI: 10.1145/87252.88081.

(60) Mack, D.; Siemssen, N.; Laufs, R. Parallel Induction by Glucose of Adherence and a Polysaccharide Antigen Specific for Plastic-Adherent Staphylococcus Epidermidis: Evidence for Functional Relation to Intercellular Adhesion. *Infect. Immun.* **1992**, *60* (5), 2048–2057.

(61) Fischer, E. R.; Hansen, B. T.; Nair, V.; Hoyt, F. H.; Dorward, D. W. Scanning Electron Microscopy. *Curr. Protoc. Microbiol.*; **2012**; 2B, 2.1-2.47. DOI: 10.1002/9780471729259.mc02b02s25.

(62) Liu, Y.; Li, G.; Fu, J.; Chen, Z.; Peng, X. Strings of Porous Carbon Polyhedrons as Self-Standing Cathode Host for High-Energy-Density Lithium–Sulfur Batteries. *Angew. Chemie - Int. Ed.* **2017**, *56* (22), 6176–6180, DOI: 10.1002/anie.201700686.

(63) Bourg, M.-C.; Badia, A.; Lennox, R. B. Gold−Sulfur Bonding in 2D and 3D Self-Assembled Monolayers: XPS Characterization. *J. Phys. Chem. B* **2000**, *104* (28), 6562–6567, DOI: 10.1021/jp9935337.

(64) Kanazawa, K. K.; Gordon, J. G. Frequency of a Quartz Microbalance in Contact with Liquid.

Anal. Chem. **1985**, *57* (8), 1770–1771, DOI: 10.1021/ac00285a062.

(65) Voinova, M. V; Rodahl, M.; Jonson, M.; Kasemo, B. Viscoelastic Acoustic Response of Layered Polymer Films at Fluid-Solid Interfaces: Continuum Mechanics Approach. *Phys. Scr.* **1999**, *59* (5), 391–396, DOI: 10.1238/Physica.Regular.059a00391.

(66) Höök, F.; Kasemo, B.; Nylander, T.; Fant, C.; Sott, K.; Elwing, H. Variations in Coupled Water, Viscoelastic Properties, and Film Thickness of a Mefp-1 Protein Film during Adsorption and Cross-Linking: A Quartz Crystal Microbalance with Dissipation Monitoring, Ellipsometry, and Surface Plasmon Resonance Study. *Anal. Chem.* **2001**, *73* (24), 5796–5804, DOI: 10.1021/ac0106501.

(67) Malmström, J.; Agheli, H.; Kingshott, P.; Sutherland, D. S. Viscoelastic Modeling of Highly Hydrated Laminin Layers at Homogeneous and Nanostructured Surfaces: Quantification of Protein Layer Properties Using QCM-D and SPR. *Langmuir* **2007**, *23* (19), 9760–9768, DOI: 10.1021/la701233y.

(68) Stewart, P. S.; Franklin, M. J. Physiological Heterogeneity in Biofilms. *Nat. Rev. Microbiol.* **2008**, *6* (3), 199–210, DOI: 10.1038/nrmicro1838.

(69) de Beer, D.; Stoodley, P.; Roe, F.; Lewandowski, Z. Effects of Biofilm Structures on Oxygen Distribution and Mass Transport. *Biotechnol. Bioeng.* **1994**, *43* (11), 1131–1138, DOI: 10.1002/bit.260431118.

(70) Izano, E. A.; Amarante, M. A.; Kher, W. B.; Kaplan, J. B. Differential Roles of Poly-N-Acetylglucosamine Surface Polysaccharide and Extracellular DNA in Staphylococcus Aureus and Staphylococcus Epidermidis Biofilms. *Appl. Environ. Microbiol.* **2008**, *74* (2), 470–476, DOI: 10.1128/AEM.02073-07.

(71) Speziale, P.; Pietrocola, G.; Foster, T. J.; Geoghegan, J. A. Protein-Based Biofilm Matrices in Staphylococci. *Front. Cell. Infect. Microbiol.* **2014**, *4*, 171, DOI: 10.3389/fcimb.2014.00171.

(72) Xiao, M.; Jasensky, J.; Foster, L.; Kuroda, K.; Chen, Z. Monitoring Antimicrobial Mechanisms of Surface-Immobilized Peptides in Situ. *Langmuir* **2018**, *34* (5), 2057–2062, DOI: 10.1021/acs.langmuir.7b03668.

(73) Brogden, K. A. Antimicrobial Peptides: Pore Formers or Metabolic Inhibitors in Bacteria? *Nat. Rev. Microbiol.* **2005**, *3* (3), 238–250, DOI: 10.1038/nrmicro1098.